

## ROLE OF SHEAR INSTABILITIES IN THE UPPER EQUATORIAL UNDERCURRENT

Hieu T. Pham<sup>1</sup>, Sutanu Sarkar<sup>2</sup>, Kraig B. Winters<sup>3</sup>

Department of Mechanical & Aerospace Engineering  
Scripps Institution of Oceanography  
University of California, San Diego  
9500 Gilman Dr., La Jolla, CA 92092

Email: h8pham@ucsd.edu<sup>1</sup>, sarkar@ucsd.edu<sup>2</sup>, kbwinters@ucsd.edu<sup>3</sup>

### ABSTRACT

A high-resolution LES model with dynamic procedure is used to investigate the role of shear instabilities on near- $N$  isopycnal oscillations and deep-cycle turbulence, the two phenomena consistently observed in the upper Equatorial Undercurrent (EUC). The model simulated at oceanographic scale has a velocity profile, which consists of a westward surface current and an eastward undercurrent, and a density profile having a surface mixed layer on top of a pycnocline, similar to the observed profiles. Results from the model indicate that a Holmboe shear instability that develops at the base of the surface mixed layer can lead to isopycnal oscillations and enhanced dissipation rate at depth in the EUC where the gradient Richardson number is greater than 0.25. The process generating turbulence consists of the primary Holmboe shear instability, secondary Kelvin-Helmholtz (KH)-like shear instability and downward vortex penetration to depths in the EUC. As the Holmboe instability grows to finite amplitude, the shear in the region immediately below the surface mixed layer is enhanced and induces secondary KH shear instability. Vortices associated with the secondary shear instability penetrate into deeper region of the EUC, are stretched the local shear and broken down into turbulence. The vortex penetrations break the oscillations down into turbulence. The dissipation rate at depth recorded during the downward penetration is larger than that seen in the surface layer. The results from the model suggest that the near- $N$  oscillations are remnants of the Holmboe shear instability and the deep-cycle turbulence is caused by secondary shear instabilities and the downward vortex penetration.

### INTRODUCTION

Turbulent mixing in the Equatorial Undercurrents (EUC) has been the focus of many field observations such as Tropic Heat I (Gregg *et al.*, 1985), Tropic Heat 2 (McPhaden & Peters, 1992), Tropical Instability Wave Experiment (Lien *et al.*, 1996) and recent campaigns in 2002 (Lien *et al.*, 2002) and 2008 (Moum *et al.*, 2011). Observational data clearly exhibits bursts of night-time deep-cycle turbulence which occur at depths far below the surface mixed layer and have an elevated dissipation rate up to three orders of magnitude larger than the value recorded during the day time at the same depth. The background flow conditions show the gradient Richardson number  $Ri_g$  exceeds

the critical value for a linear shear instability,  $Ri_{g,c} = 0.25$ , at these depths. Furthermore, the deep-cycle turbulence is shown to be strongly correlated with a narrowband near- $N$  isotherm oscillations. The generation of the oscillations is believed to be either downward propagating internal waves excited by dynamics at the base of the surface mixed layer or an occasional shear instability local to the EUC.

The strong correlation between the oscillations and the deep-cycle turbulence presumably suggests that the breakdown of the oscillations, regardless to how they are generated, leads to the enhanced mixing in the EUC. Although several numerical simulations (Skylivingstad & Denbo, 1994; Wang *et al.*, 1998; Wang & Muller, 2002; Smyth & Moum, 2002) have been performed, a physical mechanism underlying the enhanced mixing has remained elusive. A recent study using direct numerical simulations of an EUC model (Pham *et al.*, 2012) indicates that, although the oscillations and turbulence are coincident, the oscillations do not directly generate the turbulence. In the study, the oscillations are the signature of a primary Holmboe shear instability that develops at the base of the mixed layer and the deep-cycle turbulence is caused by the penetration of the vortices associated to instabilities secondary to the Holmboe shear instability. Nevertheless, since the study was done using direct numerical simulation, the simulated scale is significantly small compared to the realistic EUC parameters.

In this paper, we report the results from a high-resolution large-eddy simulation (LES) of an EUC model at an oceanographic scale to illustrate the evolution of shear instabilities which lead to both the near- $N$  oscillations and deep-cycle turbulence in the EUC. Specifically, characteristics of the oscillations and the deep-cycle turbulence from the model are shown to be consistent with the observational data. In the model, the deep-cycle turbulence is induced by a cascade of shear instabilities while the oscillations are remnants of the primary Holmboe shear instability. The mechanistic description of the evolution of shear instabilities from our EUC model provides important insights to the parameterization of the equatorial turbulence.

### MODEL FORMULATION

The model assumes a background flow condition as shown in Fig. 1, which is consistent with the observation data of the upper EUC reported in Moum *et al.* (2011).

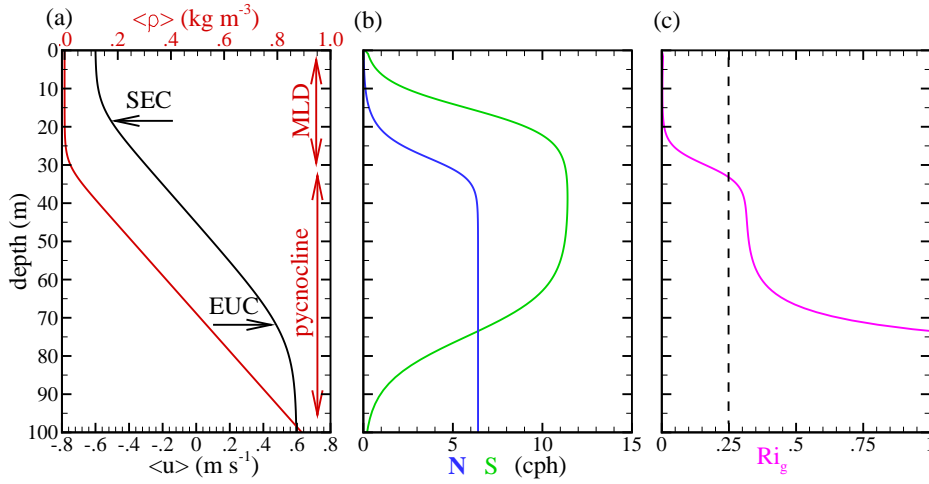


Figure 1. Initial background flow condition: (a) zonal velocity  $\langle u \rangle$  and density  $\langle \rho \rangle$  (reference density  $\rho_0 = 1000 \text{ kg m}^{-3}$  is removed); (b) buoyancy frequency  $N$  and shear  $S$ ; and (c) gradient Richardson number  $Ri_g$ . The vertical dash line in (c) denotes the critical value for a shear instability  $Ri_{g,c} = 0.25$ .

The zonal velocity  $u$  consists of the South Equatorial Current (SEC) with an easterly surface velocity of  $0.6 \text{ m s}^{-1}$  laying on top of the EUC with a peak eastward velocity of  $0.6 \text{ m s}^{-1}$  at  $100 \text{ m}$  depth. The density  $\rho$  is constructed with a mixed layer depth (MLD) of  $30 \text{ m}$  below which the density is stratified with a constant buoyancy frequency  $N = 6.4 \text{ cph}$ . The resulting profile of gradient Richardson number  $Ri_g$  shown in Fig. 1(c) shows values larger than 0.25 in the EUC. The model assumes a quiescent free-slip surface and neglects the effects of surface forcing (wind stress and buoyancy flux) and meridional velocity. Linear stability analysis using the profiles in Fig. 1 predicts a shear instability with the eigenfunction of the zonal velocity having a peak near the MLD. The present simulation aims to depict how this instability leads the near- $N$  oscillations and the deep-cycle turbulence in the EUC.

The governing equations for the zonal velocity  $u$ , meridional velocity  $v$ , vertical velocity  $w$  and density deviation  $\rho$  (deviated from a reference density  $\rho_0 = 1000 \text{ kg m}^{-3}$ ) are the three-dimensional Boussinesq equations for stratified flows with a LES subgrid model. They take the following form:

$$\frac{\partial u_i}{\partial x_i} = 0, \quad (1)$$

$$\frac{\partial u_i}{\partial t} + \frac{\partial}{\partial x_j} (u_i u_j) = -\frac{1}{\rho_0} \frac{\partial P}{\partial x_i} - \frac{g \rho \delta_{i,3}}{\rho_0} + v \frac{\partial^2 u_i}{\partial x_j \partial x_j} - \frac{\partial \tau_{ij}}{\partial x_j}, \quad (2)$$

$$\frac{\partial \rho}{\partial t} + \frac{\partial}{\partial x_j} (\rho u_j) = \kappa \frac{\partial^2 \rho}{\partial x_j \partial x_j} - \frac{\partial Q_j}{\partial x_j}. \quad (3)$$

Here,  $\nu$  and  $\kappa$  are the molecular viscosity and thermal diffusivity of water, respectively. The subgrid stress  $\tau_{ij}$  and subgrid buoyancy flux  $Q_j$  are parametrized using a dynamic Smagorinsky model as follows:

$$\tau_{ij} = \nu_{sgs} S_{ij} = -C_d \Delta^2 |S| S_{ij},$$

$$Q_j = \kappa_{sgs} \partial \rho / \partial x_j,$$

where  $S_{ij}$  is the strain rate. In the present model, we set

the subgrid viscosity  $\nu_{sgs}$  and the subgrid diffusivity  $\kappa_{sgs}$  equal so that the subgrid Prandtl number  $Pr_{sgs} = \nu_{sgs} / \kappa_{sgs}$  is unity. The filter width  $\Delta$  is taken to be  $(\Delta x \Delta y \Delta z)^{1/3}$ . Following Germano *et al.* (1991), the model coefficients  $C_d$  is determined by a dynamic procedure in which a test filter is applied to the resolved velocity fields. The dynamic coefficient is computed as:

$$C_d = -\frac{1}{2} \frac{\langle L_{ij} M_{ij} \rangle}{\langle M_{ij} M_{ij} \rangle},$$

where  $L_{ij} = \widehat{u_i u_j} - \widehat{u_i} \widehat{u_j}$ , and  $M_{ij} = \widehat{\Delta^2 |S| S_{ij}} - \Delta^2 |S| S_{ij}$ . Quantities denoted  $\widehat{\cdot}$  are test-filtered using a 2<sup>nd</sup>-order top hat filter.

Second-order finite difference in space and third-order Runge-Kutta marching in time are used to integrate (Eqs. 1-3). The computational domain consists of  $768 \text{ m}$  in the zonal ( $x$ ) direction,  $48 \text{ m}$  in the meridional ( $y$ ) direction and  $360 \text{ m}$  in the vertical ( $z$ ) direction. The domain is discretized at  $1 \text{ m}$  resolution in the horizontal directions while the vertical grid is stretched using 384 gridpoints at a spacing as fine as  $10 \text{ cm}$  at the MLD. The model assumes periodicity in the horizontal directions and a sponge layer is employed in region between depths of  $200 \text{ m}$  and  $360 \text{ m}$  to prevent internal waves to reflect from the bottom boundary into the EUC. Broadband velocity perturbations with amplitude of  $0.012 \text{ m s}^{-1}$  are added to initiate the shear instability. In our discussion, a mean quantity denoted by angle brackets  $\langle \cdot \rangle$  is the horizontally-averaged value and a fluctuating quantity is the deviation from the mean and denoted by prime  $\prime$ . The model is simulated for a duration of 6 hours.

## ISOPYCNAL OSCILLATIONS AND DEEP-CYCLE TURBULENCE

Results from the model show presence of the near- $N$  isopycnal oscillations and the deep-cycle turbulence far below the MLD where the initial (at  $t = 0$ ) horizontally-average  $Ri_g$  is larger than the critical value of 0.25. The characteristics of the oscillations and the turbulence is consistent with the observational data. Isopycnal oscillations

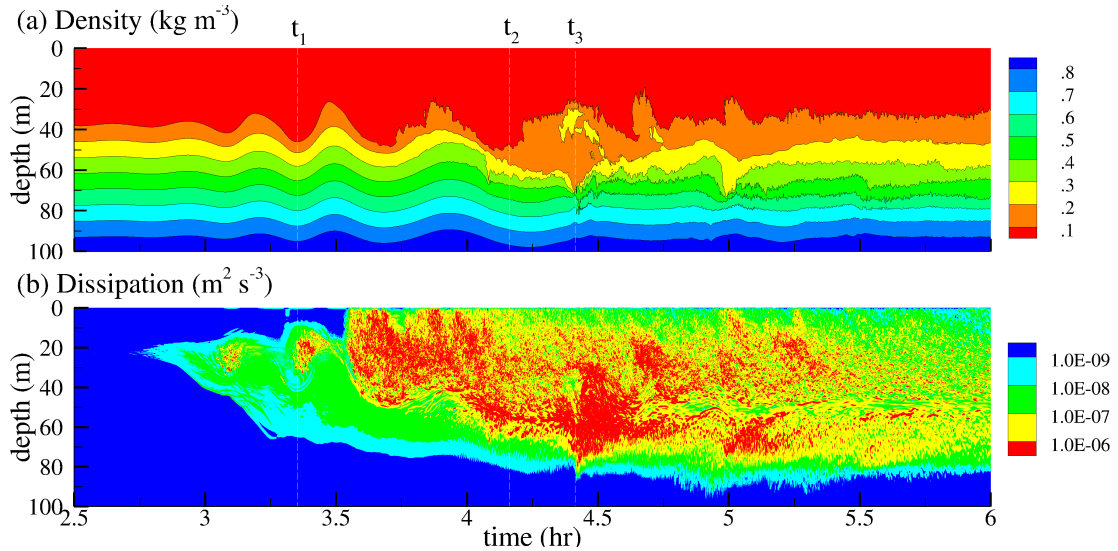


Figure 2. (a) Isopycnal oscillations and (b) deep-cycle turbulence between 30m and 100m depth in the EUC recorded along a vertical pencil at  $x = 385m$  and  $y = 24m$ .

begin to develop near the MLD at time  $t = 3hr$  as shown in Fig. 2(a). Vertically-coherent in-phase oscillations can be seen at 100m depth. The oscillations propagate westward at a speed  $c = 0.4ms^{-1}$ , which is approximately equal to the background velocity  $\langle u \rangle$  at 25m depth. At  $t = 3.75hr$ , the oscillations near the MLD at depths of 30–40m grow to finite amplitude and transition into turbulence. The oscillations in the EUC at depths of 80–100m also grow to larger amplitude but they do not evolve into turbulence as in the surface mixed layer. Approximately at  $t = 4hr$ , turbulence spreads from the MLD into the EUC and the oscillations in the EUC disappear. The isopycnal fluctuations at frequencies much higher than that of the oscillations dominates the region between depths of 40–80m.

An elevated dissipation rate is seen in the surface mixed layer at time  $t = 3hr$  as shown in Fig. 2(b). The dissipation rate is also high in the region between depths of 30m and 80m during  $t = 4hr$  and 6hr with the value as high as  $10^{-5}m^2s^{-3}$ . In our model, the dissipation rate  $\varepsilon$  is composed of a resolved component,  $\langle 2vS'_{ij}S'_{ij} \rangle$  and a sub-grid component,  $\langle -\tau'_{ij}S'_{ij} \rangle$ , with the latter dominating the total dissipation rate. The magnitude of dissipation seen in our model is consistent with the values reported by Moum *et al.* (1992), Lien *et al.* (2002) and Moum *et al.* (2011). It is noted that in time the dissipation spreads from the MLD downward into the EUC in bursts. For example, in a short duration from  $t = 4hr$  to 4.1hr, the dissipation spreads from 40m to 60m depth as shown in Fig. 2(b) and the isopycnal oscillations disappear from this region as in Fig. 2(a). The isopycnals are flattened after the burst without any evidence of an overturn. Between  $t = 4.25hr$  and 4.5hr, an overturn with intense dissipation rate occurs between depths of 30–60m with the isopycnal displacement significantly larger than the amplitude of the oscillations seen at earlier time. It is important to emphasize that the oscillatory isopycnals between depths of 40m and 60m have disappeared for nearly half an hour prior to the onset of the overturn. In our model, the deep-cycle turbulence is *not* directly related to the overturn of the oscillations in the EUC in contrast to the discussion in Hebert *et al.* (1992).

In Figs. 3(a) and 3(c), we plot the time evolution of

the density and the dissipation rate, respectively, at 5 different depths in the EUC, similar to observed data collected by a mooring. Several cycles of the oscillations are clearly seen at all depths between  $t = 2.5hr$  and 4hr. The frequency of the oscillations has a range between 3–4cph as shown in Fig. 3(b), which is close to the value of the background buoyancy frequency  $N = 6.4cph$ . The near- $N$  frequency agrees well with the observations in Lien *et al.* (2002) and Moum *et al.* (2011). Higher-frequency fluctuations are observed later in time accompanied with an elevation in the dissipation rate. The two-order-of-magnitude elevation (from  $10^{-10}$  to  $10^{-8}m^2s^{-3}$ ) in the dissipation rate occurs first at 30m depth and spreads downward to greater depths. Different from Smyth *et al.* (2011) who suggest that the deep-cycle turbulence is due to an occasional isolated shear instability happening at depths in the EUC, our model indicates that the turbulence actually descends downward in a sequence of instabilities from the base of the surface mixed layer. When the oscillations disappear, the dissipation rate reaches up to  $10^{-5}m^2s^{-3}$  at all depths. At  $t = 4.8hr$ , the top four density records converge signifying an event of intense mixing. Also, at this time, the density at 70m depth shows a sudden spike to lower value indicating that lighter fluid from the upper region is pushed down to this depth. When the spike occurs, the density oscillations seen earlier disappear and the dissipation rate is elevated by two orders of magnitude. Another spike in the density and dissipation rate is seen at this depth at  $t = 5hr$ . Vertical profiles of turbulent heat flux show significant mixing with peak values occurring in the EUC. Value of the fluxes in our model is up to  $150Wm^{-2}$  which also agrees with the value reported in Moum *et al.* (2011).

## ROLE OF SHEAR INSTABILITIES

The oscillations and the deep-cycle turbulence in our model result from a series of shear instabilities originating from the base of the mixed layer. Figs. 4(a-c) show snapshots of the density field at three times marking as  $t_1$ ,  $t_2$  and  $t_3$  in Figs. 2 and 3 to illustrate how shear instabilities can generate near- $N$  oscillations and deep-cycle turbulence as observed in the EUC.

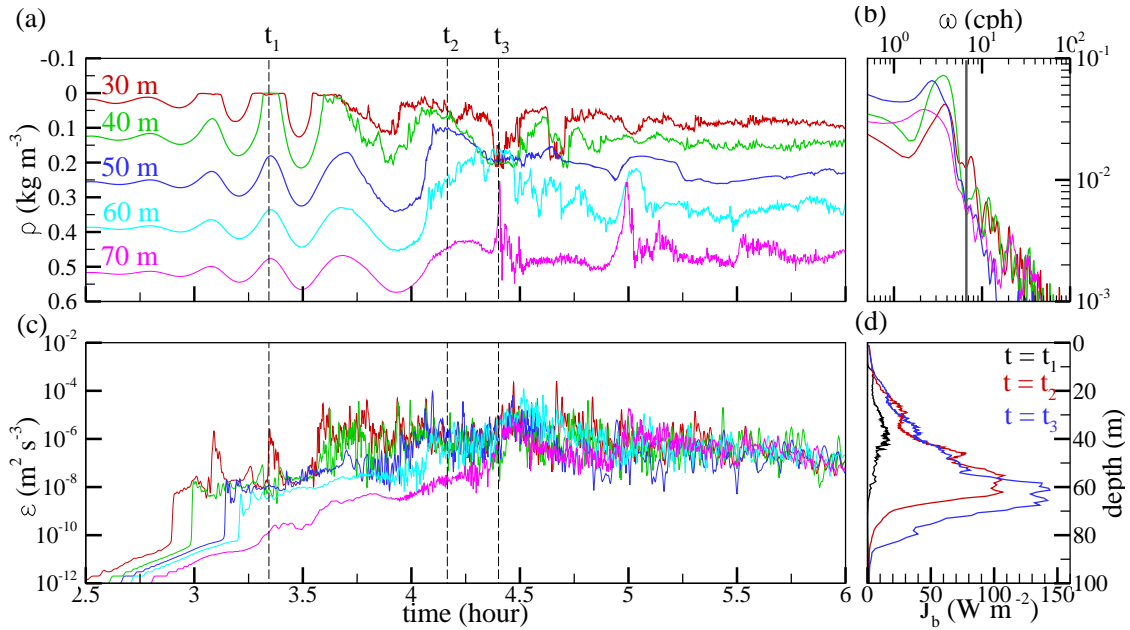


Figure 3. Time evolution of (a) the density and (c) the dissipation rate at 5 depths in the EUC at a fixed horizontal location  $x = 385m$  and  $y = 24m$ ; (b) the frequency spectra of the isopycnal oscillations shown in (a), the vertical solid line indicates the buoyancy frequency  $N$  in the EUC; (d) Vertical profiles of horizontally-averaged turbulent heat fluxes at  $J_b$  at three times denoted in (a).

At time  $t_1$ , a Holmboe shear instability develops at the base of the surface mixed layer where the gradient Richardson number is less than 0.25 as shown in Fig. 4(a). The instability has a zonal wavelength of 384m and a westward phase speed of  $0.4ms^{-1}$ . The instability grows to form wisps with the vertical scale as large as the MLD in the surface layer. At the same time, the instability causes the isopycnal oscillations having the same wavelength and phase speed in the EUC. The westward direction, the phase speed and the wavelength in our model fall in range with the estimation from observational data (Lien *et al.*, 2002; Moum *et al.*, 2011). Linear stability analyses of Sun *et al.* (1998) and Smyth *et al.* (2011) also support the notion that a shear instability can generate oscillations in the isopycnals in the region deeper than where the instability first occurs.

At time  $t_2$ , the wisps generated by the Holmboe instability in the mixed layer have broken down, and a secondary shear instability develops at 50m depth where the gradient Richardson number is less than 0.25. This shear instability induces an isopycnal overturn, similar to a Kelvin-Helmholtz (KH) billow, with a vertical scale of approximately 20m which is significantly smaller than the wisps caused by the primary Holmboe instability. The gradient Richardson number between 40m and 60m depths has decreased between time  $t_1$  and  $t_2$ . The reduction is due to a larger shear rate induced by the growth to finite amplitude of the Holmboe instability. The induction of secondary shear instability is also observed in the scale-down model of the EUC in a direct numerical simulation (Pham *et al.*, 2012).

At time  $t_3$ , a vortex associated with the overturn seen at  $t_2$  impinges downward to 80m depth. It is stretched eastward by the EUC shear and broken down into turbulence. It is the vortex penetration that destroys the oscillations in the EUC. In our model, the oscillations in the EUC do not overturn to give rise to the deep-cycle turbulence as hypothesized in previous literature (Moum *et al.*, 1992; Lien *et al.*, 2002). The penetration and stretching of vortices by an am-

bient EUC shear has been seen previously in Pham & Sarkar (2010). The penetration obstructs the zonal flow in the EUC which results in an isopycnal overturn with a vertical scale of approximately 40m. The size of this overturn is significantly larger than those caused by the Holmboe instability and secondary shear instability. Over the simulation, the dissipation rate and the turbulent heat flux recorded during the overturn are most intense as shown in Figs. 3(c,d).

Our model indicates that both the near- $N$  oscillations and the deep-cycle turbulence result from a Holmboe shear instability that develops at the base of the surface mixed layer. The development of a secondary KH-like shear instability and the subsequent vortex penetrations triggers the deep-cycle turbulence at greater depths in the EUC. It is important to examine the role of each of these physics in term of the turbulent kinetic energy (TKE) budget. For the present model, the evolution of the TKE budget is described by following equation:

$$\frac{dK}{dt} = P - \varepsilon + B - \frac{dT_3}{dz} - \frac{dT_{3,sgs}}{dz}, \quad (4)$$

where,  $K = 1/2 \langle u'_i u'_i \rangle$  is the TKE,  $P = -\langle u'w' \rangle d\langle u \rangle / dz$  is the production rate, and  $\varepsilon$  is previously defined total dissipation rate. The buoyancy flux is defined as  $B = -g/\rho_0 \langle p'w' \rangle$ . The transport  $T_3$  and subgrid transport  $T_{3,sgs}$  are computed as  $1/2 \langle w' u'_i u'_i \rangle + \langle p'w' \rangle / \rho_0 - 2\nu \langle u'_i S'_{3i} \rangle$ , and  $\langle \tau'_{3i} u'_i \rangle$ , respectively. Figs. 5(a-c) show the terms in the budgets at times  $t_1$ ,  $t_2$ , and  $t_3$ , respectively. The subgrid transport is significantly smaller than the other terms, and, is not plotted.

At time  $t_1$  when the Holmboe shear instability has developed, the balance in the budget above the 40m depth is different from that in the region below as shown in Fig. 5(a). The dissipation is only large above 40m depth due to the mixing in the wisps of the Holmboe waves. The production is also large above this depth but extends down to 80m

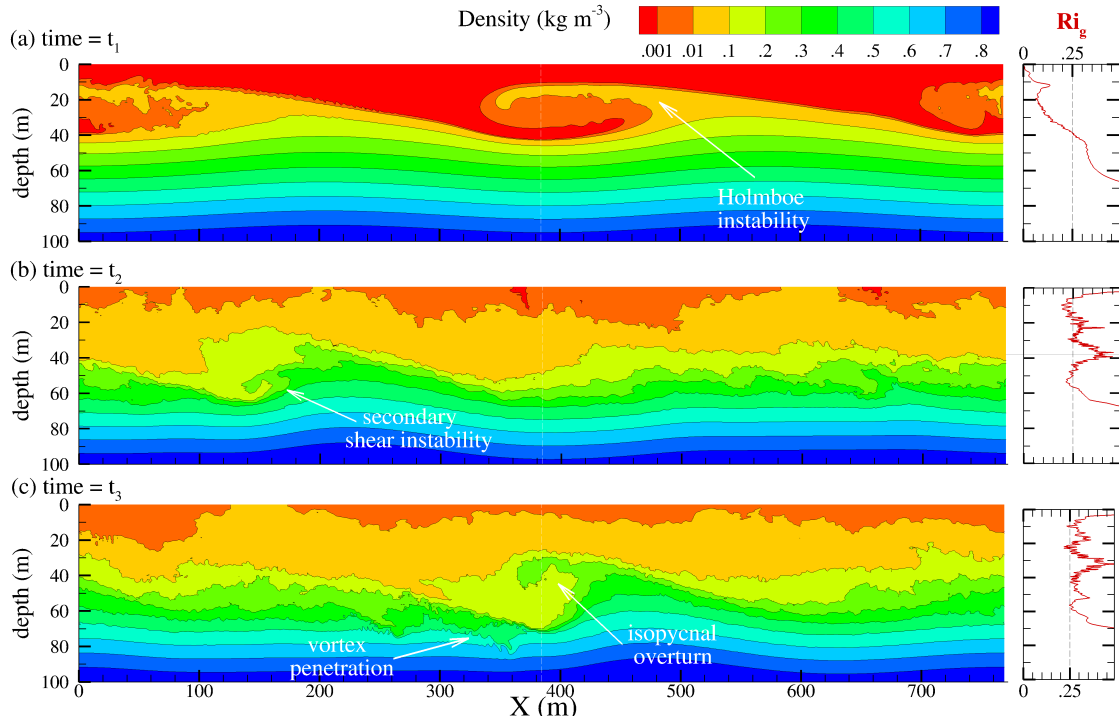


Figure 4. Spatial structures of Holmboe and secondary shear instabilities in a vertical  $x-z$  slice of the density field at  $y = 24\text{ m}$  at times  $t_1$ ,  $t_2$  and  $t_3$  denoted in Fig. 2 and 3. White dash lines denote location of the vertical pencil where data is plot in those figures. Panels to the right plot instantaneous horizontally-averaged gradient Richardson number,  $Ri_g$ , with the black lines indicating the critical value,  $Ri_{g,c} = 0.25$ .

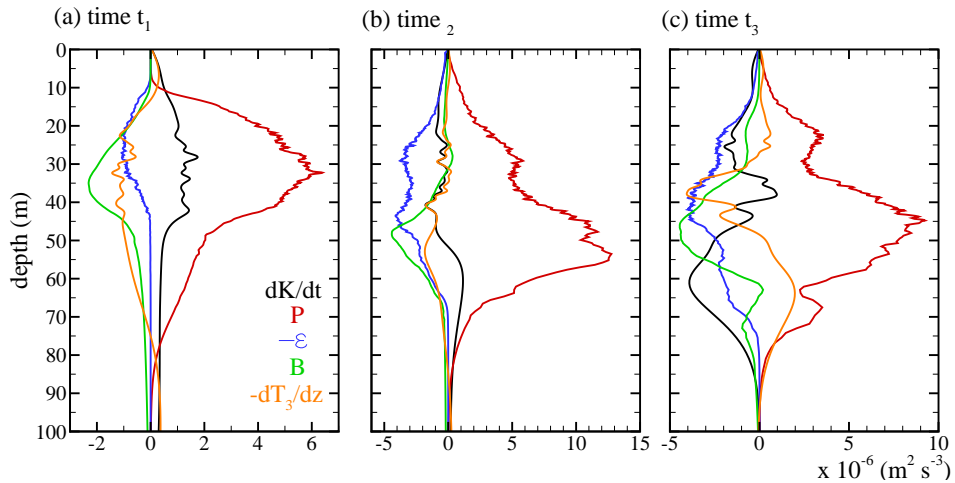


Figure 5. Budgets at times  $t_1$ ,  $t_2$  and  $t_3$  shows the sources and sinks of the turbulent kinetic energy as the deep-cycle turbulence descends from the surface layer down into the EUC.

depth. The extension to greater depths is also seen in the buoyancy flux and transport. The production at depth is not due to turbulence but it is a result of the near- $N$  oscillations advecting in a stratified background with shear. When the Holmboe instability develops, it generates a downward momentum flux  $\langle u'w' \rangle$  into the EUC region with shear. The combination of this momentum flux and the EUC shear causes profiles of the production, buoyancy flux and transport to extend down to the core of the EUC. The energy associated with the momentum flux does not generate turbulence since there is no dissipation. The transport is dominated by the pressure velocity correlation, not the triple turbulent velocity correlation. The energy in this region is converted back and forth between the forms of fluctuating

kinetic energy and fluctuating potential energy as in a wave.

At time  $t_2$  as the secondary shear instability and downward vortex penetration have occurred, the dissipation descends down to  $70\text{ m}$  depth as shown in Fig. 5(b). The production at this time peaks at  $55\text{ m}$  depth at a value significantly larger than that seen earlier at  $t_1$ . The turbulence transported downward by the vortices interacts with the marginally-stable EUC shear to generate more turbulence production. It is important to emphasize the two types of production between time  $t_1$  and  $t_2$  in this region of the EUC between depths of  $40\text{ m}$  and  $80\text{ m}$ . At time  $t_1$ , this region has large production and negligible dissipation, so the production is wave production as in Pham & Sarkar (2010). In contrast, both the production and dissipation are large at time

August 28 - 30, 2013 Poitiers, France

$t_2$ , so the production is associated with turbulence. Wave production does not mix the momentum and density in the ambience as turbulent production does. At time  $t_3$ , turbulence dominates the entire EUC region below 40m depth. The transport, which is negative at times  $t_1$  and  $t_2$ , is positive at this time denoting an upward energy flux. The upward transport is dominated by the turbulent triple velocity correlation, not by the pressure velocity correlation as seen at earlier times.

## CONCLUSIONS

Using a LES model of an upper Equatorial Undercurrent at oceanographic scale, we have illustrated in detail the mechanistic process of how a shear instability at the base of the surface mixed layer can lead to the near- $N$  oscillations and the deep-cycle turbulence in the EUC. The 384m oscillations having a frequency of 3–4cph and the enhanced dissipation rate with the magnitude up to  $10^{-5}m^2s^{-3}$  in our model agree well with the observational data reported in previous literature. In the model, the oscillations are remnant-at-depth of a shear instability that develops at the base of the surface mixed layer where the gradient Richardson number is less than 0.25. When this primary instability grows to finite amplitude, it enhances the shear rate in the EUC. In effect, the local gradient Richardson number is reduced such that a secondary shear instability is induced. Vortices associated with the secondary shear instability penetrate downward, destroy the oscillations and obstruct the flow in the deeper region. The obstruction causes large-amplitude isopycnal overturns which results in elevated dissipation rate. Our model suggests that the deep-cycle turbulence results from a series of shear instabilities and vortex penetrations, not a direct overturn of the oscillations.

Our model depicts an evolutionary process in which one shear instability can trigger another shear instability which in turn can induce other processes. These complicated mechanism can not be parameterized using a  $Ri_g$ -based scheme in which the type of the shear instabilities is not even identified. The turbulence generation by a KH shear instability is different from that by a Holmboe instability (Smyth & Winters, 2003), and therefore, different parameterization scheme is needed for each type. When the secondary shear instabilities in our model develop, the gradient Richardson number is less than 0.25. It is difficult to identify its type if one purely looks at the vertical profile of the gradient Richardson number. An incorrect identification of this secondary shear instability as a Holmboe shear instability would mistreat the horizontal scale of the overturns by an order-of magnitude. Finally, the large-scale overturns induced by the vortex penetrations occur when the gradient Richardson number is larger than 0.25; parameterization using a  $Ri_g$ -based scheme would not be able to detect such mixing. In order to parameterize the processes depicted in our model into large-scale ocean model, a more sophisticated scheme is needed.

## REFERENCES

- Germano, M., Piomelli, U., Moin, P. & Cabot, W. 1991 A dynamic subgrid-scale eddy viscosity model. *Phys. Fluids* **3**, 1760–1765.
- Gregg, M. C., Peters, H., Wesson, J. C., Oakey, N. S. & Shay, T. J. 1985 Intensive measurements of turbulence and shear in the Equatorial Undercurrent. *Nature* **314** (14), 140–144.
- Hebert, D., Moum, J., Paulson, C. & Caldwell, D. 1992 Turbulence and internal waves at the equator. Part II: Details of a single event. *J. Phys. Oceanogr.* **22**, 1346–1356.
- Lien, R.-C., D'Asaro, E. & McPhaden, M. 2002 Internal waves and turbulence in the upper central equatorial Pacific: Lagrangian and Eulerian observations. *J. Phys. Oceanogr.* **32**, 2619–2639.
- Lien, R.-C., McPhaden, M. & Gregg, M. 1996 High-frequency internal waves at  $0^\circ$ ,  $140^\circ$  W and their possible relationship to deep-cycle turbulence. *J. Phys. Oceanogr.* **26**, 581–600.
- McPhaden, M. & Peters, H. 1992 Diurnal cycle of internal wave variability in the equatorial Pacific ocean: Results from moored observations. *J. Phys. Oceanogr.* **22**, 1317–1329.
- Moum, J., Hebert, D., Paulson, C. & Caldwell, D. 1992 Turbulence and internal waves at the equator. Part I: Statistics from towed thermistors and a microstructure profiler. *J. Phys. Oceanogr.* **22**, 1330–1345.
- Moum, J. N., Nash, J. D. & Smyth, W. D. 2011 Narrow-band oscillations in the upper equatorial ocean. Part I: Interpretation as shear instabilities. *J. Phys. Oceanogr.* **41**, 397–410.
- Pham, H. T. & Sarkar, S. 2010 Internal waves and turbulence in a stable stratified jet. *J. Fluid Mech.* **648**, 297–324.
- Pham, H. T., Sarkar, S. & Winters, K. B. 2012 Near- $n$  oscillations and deep-cycle turbulence in an upper Equatorial Undercurrent model. *J. Phys. Oceanogr.* **42**, 2169–2184.
- Skyllingstad, E. & Denbo, D. 1994 The role of internal gravity waves in the equatorial current system. *J. Phys. Oceanogr.* **24**, 2093–2110.
- Smyth, W. & Moum, J. 2002 Shear instability and gravity wave saturation in an asymmetrically stratified jet. *Dyn. Atmos. Oceans* **35**, 265–294.
- Smyth, W. D., Moum, J. N. & Nash, J. D. 2011 Narrow-band oscillations at the upper equatorial ocean. Part II: Properties of shear instabilities. *J. Phys. Oceanogr.* **41**, 412–428.
- Smyth, W. D. & Winters, K. B. 2003 Turbulence and mixing in Holmboe waves. *J. Phys. Oceanogr.* **33**, 694–711.
- Sun, C., Smyth, W. D. & Moum, J. 1998 Dynamic instability of stratified shear flow in the upper equatorial Pacific. *J. Geophys. Res.* **103**, 10323–10337.
- Wang, D., McWilliams, J. & Large, W. 1998 Large-eddy simulation of the diurnal cycle of deep equatorial turbulence. *J. Phys. Oceanogr.* **28**, 129–148.
- Wang, D. & Muller, P. 2002 Effects of equatorial undercurrent shear on upper-ocean mixing and internal waves. *J. Phys. Oceanogr.* **32**, 1041–1057.